Dissipation in the $1/D$ expansion for planar matrix models

Takanori Anegawa,[1,*] Norihiro Iizuka,[2,3,†] and Daniel Kabat[4,5,‡]

[1]*Yonago College, National Institute of Technology, Yonago, Tottori 683-8502, Japan*
[2]*Department of Physics, National Tsing Hua University, Hsinchu 300044, Taiwan*
[3]*Yukawa Institute for Theoretical Physics, Kyoto University, Kyoto 606-8502, Japan*
[4]*Department of Physics and Astronomy, Lehman College, City University of New York, 250 Bedford Park Boulevard West, Bronx, New York 10468, USA*
[5]*Graduate School and University Center, City University of New York, 365 Fifth Avenue, New York, New York 10016, USA*

(Received 19 October 2024; accepted 1 December 2024; published 6 January 2025)

We consider the thermal behavior of a large number of matrix degrees of freedom in the planar limit. We work in $0+1$ dimensions, with D matrices, and use $1/D$ as an expansion parameter. This can be thought of as a noncommutative large-D vector model, with two independent quartic couplings for the two different orderings of the matrices. We compute a thermal two-point correlator to $\mathcal{O}(1/D)$ and find that the degeneracy present at large D is lifted, with energy levels split by an amount $\sim 1/\sqrt{D}$. This implies a timescale for thermal dissipation $\sim\sqrt{D}$. At high temperatures dissipation is predominantly due to one of the two quartic couplings.

DOI: 10.1103/PhysRevD.111.025003

I. THE MODEL

Consider the quantum mechanics of a collection of $N \times N$ Hermitian matrices $X^i(\tau)$, $i = 1, \ldots, D$. We describe them using a Euclidean action

$$S = \int d\tau \frac{1}{2}\mathrm{Tr}(\partial_\tau X^i \partial_\tau X^i) + \frac{1}{2}m_0^2 \mathrm{Tr}(X^i X^i) + \frac{1}{2}g_A^2 \mathrm{Tr}(X^i X^i X^j X^j) - \frac{1}{2}g_C^2 \mathrm{Tr}(X^i X^j X^i X^j). \quad (1)$$

Here m_0 is a bare mass parameter, and we have introduced two quartic couplings g_A, g_C.

We will study the model (1) for its own sake. However, as motivation note that if we set $m_0 = 0$ and $g_A = g_C = g_{\mathrm{YM}}$ then the action reduces to

$$S = \int d\tau \frac{1}{2}\mathrm{Tr}(\partial_\tau X^i \partial_\tau X^i) - \frac{1}{4}g_{\mathrm{YM}}^2 \mathrm{Tr}([X^i, X^j]^2). \quad (2)$$

Although the model we consider has no gauge symmetry, the same potential term appears in the dimensional reduction of $U(N)$ Yang-Mills theory from $D+1$ to $0+1$ dimensions. The commutator-squared potential is also familiar in the Banks-Fischler-Shenker-Susskind matrix model [1]. In the model (1) we treat g_A and g_C as independent couplings since, as we will see, they lead to rather different dynamics.

We are interested in the leading large-N limit, in which only planar diagrams contribute. However, we are also interested in the behavior for large D. So instead of holding the two 't Hooft couplings fixed, we instead consider the limit

$$\lambda_A = g_A^2 N \to 0 \quad \text{with} \quad \tilde{\lambda}_A = \lambda_A D \quad \text{fixed},$$
$$\lambda_C = g_C^2 N \to 0 \quad \text{with} \quad \tilde{\lambda}_C = \lambda_C D \quad \text{fixed}. \quad (3)$$

Our goal is to study dissipation in this model at large D. That is, we are interested in dissipation in a many-matrix model. This is a tractable problem because the model has an $SO(D)$ symmetry that acts on the i, j indices, and from that point of view it is similar to a large-D vector model and we can use $1/D$ as an expansion parameter. However, from the $U(N)$ point of view we are restricting to planar diagrams, which means it is *not* a standard vector model. Instead (1) defines a sort of "noncommutative" vector model, which lets us distinguish between the two couplings g_A and g_C. Another perspective on the model is to think of X^i_{AB} as a three-index object, which means we are dealing with a tensor model [2] in a particular scaling limit. A different scaling limit was considered in [3,4]. In the literature the $1/D$ expansion has been developed to study correlation functions [5] and the thermal partition function [6], and it has been applied to a commuting vector model in [7]. Related techniques were used to study Lyapunov exponents in scalar field theory in [8].

*Contact author: takanegawa@gmail.com
†Contact author: iizuka@phys.nthu.edu.tw
‡Contact author: daniel.kabat@lehman.cuny.edu

II. HUBBARD-STRATONOVICH APPROACH

A. Hubbard-Stratonovich transformation

To proceed it is convenient to perform a Hubbard-Stratonovich transformation and introduce an auxiliary Hermitian field Σ,

$$S = \int d\tau \frac{1}{2}\mathrm{Tr}(\partial_\tau X^i \partial_\tau X^i) + \frac{1}{2}m_0^2 \mathrm{Tr}(X^i X^i) + \frac{1}{2}\mathrm{Tr}(\Sigma^2) - ig_A \mathrm{Tr}(\Sigma X^i X^i) - \frac{1}{2}g_C^2 \mathrm{Tr}(X^i X^j X^i X^j). \tag{4}$$

The Gaussian path integral over Σ is well defined, and the saddle point fixes $\Sigma = ig_A X^i X^i$. Integrating out Σ using its algebraic equation of motion recovers (1).[1] This is a standard step for large-D vector models and as we will see it is the most convenient way to treat the coupling g_A. We set

$$\Sigma = \Sigma_0 \mathbb{1}_{N\times N} + \sigma \qquad m^2 = m_0^2 - 2ig_A\Sigma_0 \tag{5}$$

so that

$$S = \int d\tau \frac{1}{2}\mathrm{Tr}(\partial_\tau X^i \partial_\tau X^i) + \frac{1}{2}m^2 \mathrm{Tr}(X^i X^i) + \frac{1}{2}\mathrm{Tr}(\sigma^2) + \Sigma_0 \mathrm{Tr}(\sigma) - ig_A \mathrm{Tr}(\sigma X^i X^i) - \frac{1}{2}g_C^2 \mathrm{Tr}(X^i X^j X^i X^j). \tag{6}$$

We choose the parameter Σ_0 so that the vacuum expectation value (VEV) of σ vanishes. This fixes[2]

$$\Sigma_0 \mathbb{1}_{N\times N} = ig_A \langle X^i X^i \rangle \tag{7}$$

or equivalently

$$\Sigma_0 = ig_A \frac{1}{N}\langle \mathrm{Tr}(X^i X^i)\rangle. \tag{8}$$

With Σ_0 fixed in this way, (5) gives an equation that fixes the mass m of the fields X^i. Note that m has been defined so that the VEV of σ vanishes. At large D it is also the location of the pole in the X^i propagator, but as we will see $1/D$ corrections to the propagator shift the location of the pole. So in general m is simply a parameter that characterizes the theory.

Before proceeding it is worth doing some dimensional analysis. For the action to be dimensionless we have

$$X^i \sim (\mathrm{mass})^{-1/2}, \qquad \sigma, \Sigma_0 \sim (\mathrm{mass})^{1/2}, \qquad g_A^2, \lambda_A, \tilde{\lambda}_A, g_C^2, \lambda_C, \tilde{\lambda}_C \sim (\mathrm{mass})^3. \tag{9}$$

[1] A more careful argument is given in Appendix A.

[2] This condition is a consequence of one of the Schwinger-Dyson equations of the model (6), namely $\langle \frac{\delta S}{\delta \sigma}\rangle = 0$ or equivalently $\langle \sigma \rangle = ig_A \langle X^i X^i \rangle - \Sigma_0 \mathbb{1}_{N\times N}$.

B. Zero-temperature results

We begin by studying the two-point functions in the model (6) at zero temperature. We do this by self-consistently solving the Schwinger-Dyson equations of the model to $\mathcal{O}(1/D)$. The condition (7) eliminates tadpoles, and as a result, the Schwinger-Dyson equations we need to solve are schematically shown in Fig. 1.

The diagrams in Fig. 1 are schematic in the sense that numerical factors have been suppressed. To proceed we introduce bare propagators [with $U(N)$ and $SO(D)$ indices suppressed]

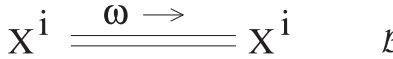

$$\mathcal{B}_X(\omega) = \frac{1}{\omega^2 + m^2} \tag{10}$$

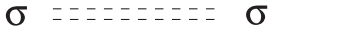

$$\mathcal{B}_\sigma(\omega) = 1 \tag{11}$$

and dressed propagators

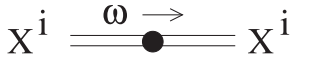

$$\mathcal{D}_X(\omega) \tag{12}$$

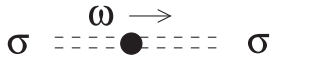

$$\mathcal{D}_\sigma(\omega). \tag{13}$$

These are related through one-particle irreducible (1PI) self-energies by

$$\mathcal{D}_X^{-1} = \mathcal{B}_X^{-1} - \mathcal{E}_X \tag{14}$$

$$\mathcal{D}_\sigma^{-1} = \mathcal{B}_\sigma^{-1} - \mathcal{E}_\sigma. \tag{15}$$

Using Fig. 1 as a guide, the diagrams that contribute to $\mathcal{E}_X$ to $\mathcal{O}(1/D)$ are shown in Fig. 2. This leads to

$$D_X^{-1}(\omega) = \omega^2 + m^2 - \Big[4g_c^2 N \int \frac{dk}{2\pi} D_X(k) - 2g_A^2 N \int \frac{dk}{2\pi} D_X(k+\omega) D_\sigma(k) + 4g_C^4 N^2 D \int \frac{dk_1}{2\pi}\frac{dk_2}{2\pi} D_X(k_1) D_X(k_2) \times D_X(k_1+k_2+\omega)\Big] \tag{16}$$

(for an explanation of numerical factors see Appendix B). Likewise the diagrams that contribute to $\mathcal{E}_\sigma$ to $\mathcal{O}(1/D)$ are shown in Fig. 3 and lead to

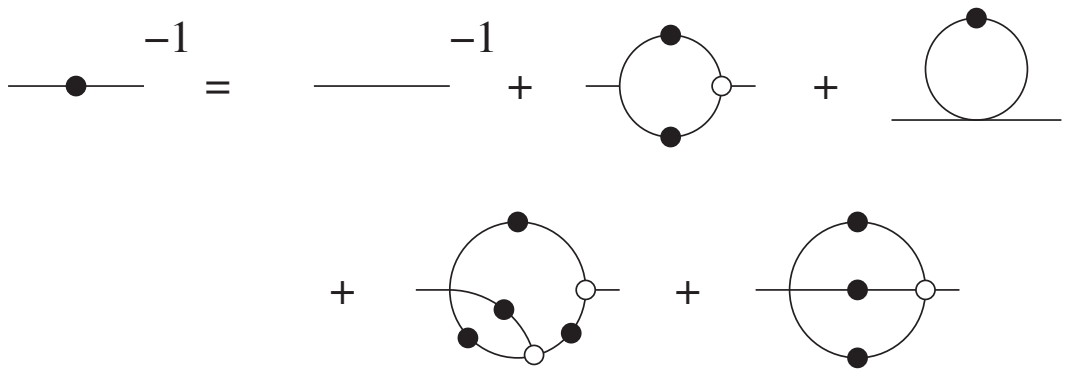

FIG. 1. Schematic form of the Schwinger-Dyson equations for a theory with three- and four-point couplings but no tadpoles. Solid blobs are dressed propagators; empty circles are 1PI vertices. In the loop diagrams all numerical factors have been suppressed and all external lines are understood to be amputated. See for example [9–12].

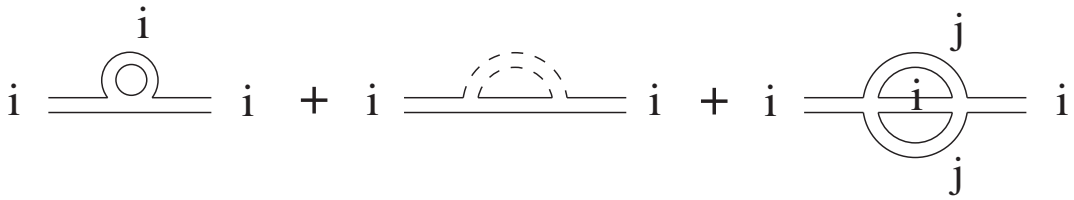

FIG. 2. Diagrams that contribute to $\mathcal{E}_X$ to $\mathcal{O}(1/D)$. Internal lines are understood to be dressed propagators, external lines are amputated. There is no sum on i, but there is a sum on j in the last diagram. In double-line notation the first two diagrams also appear in the flipped forms 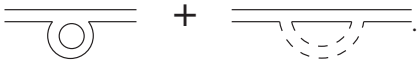 .

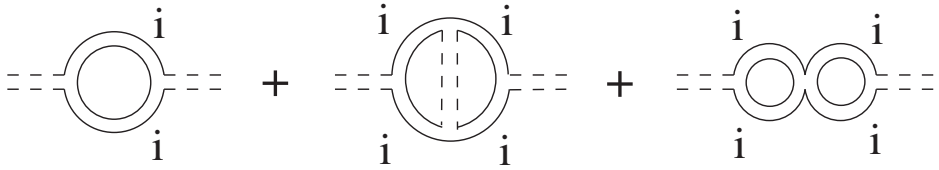

FIG. 3. Diagrams that contribute to $\mathcal{E}_\sigma$ to $\mathcal{O}(1/D)$. Internal lines are understood to be dressed propagators, external lines are amputated. There is a sum over the vector index i.

$$D_\sigma^{-1}(\omega) = 1 - \left[-g_A^2 N D \int \frac{dk}{2\pi} D_X(k) D_X(k+\omega) + 2 g_A^4 N^2 D \int \frac{dk_1}{2\pi}\frac{dk_2}{2\pi} D_X(k_1) D_X(k_2) D_\sigma(k_1-k_2) D_X(k_1+\omega) D_X(k_2+\omega) \right.$$
$$\left. - 2 g_A^2 g_C^2 N^2 D \int \frac{dk_1}{2\pi}\frac{dk_2}{2\pi} D_X(k_1) D_X(k_2) D_X(k_1+\omega) D_X(k_2+\omega) \right]. \tag{17}$$

Since we have $1/D$ as an expansion parameter it is quite easy to solve these equations. At leading order for large D, the only contribution to the self-energies comes from the first term (the bubble term) in $\mathcal{E}_\sigma$. This means that at leading order for large D we have

$$D_\sigma^{-1}(\omega) = 1 + \tilde{\lambda}_A \int \frac{dk}{2\pi} \frac{1}{k^2+m^2} \frac{1}{(k+\omega)^2+m^2}$$
$$= 1 + \frac{\tilde{\lambda}_A}{m(\omega^2+4m^2)}. \tag{18}$$

Thus,

$$D_\sigma = \frac{\omega^2 + 4m^2}{\omega^2 + m_\sigma^2} \tag{19}$$

where we have defined

$$m_\sigma^2 = 4m^2 + \tilde{\lambda}_A/m. \tag{20}$$

We use this result to evaluate the loop integrals in the X^i self-energy to $\mathcal{O}(1/D)$. The integrals in (16) lead to

$$D_X^{-1}(\omega) = \omega^2 + m^2 - \frac{4\tilde{\lambda}_C}{2mD} + \frac{\tilde{\lambda}_A}{mD}\frac{\omega^2 + 5m^2 + mm_\sigma + 4m^3/m_\sigma}{\omega^2 + (m + m_\sigma)^2} - \frac{3\tilde{\lambda}_C^2}{m^2 D}\frac{1}{\omega^2 + 9m^2}. \tag{21}$$

We can evaluate the self-energy on shell, by setting the Euclidean momentum to $\omega^2 = -m^2$. We see that the self-energy is real and to $\mathcal{O}(1/D)$ the only effect is a small shift in the physical (pole) mass of the fields X^i.

We can also determine the relation between the parameter m and the bare parameters of the model (1). The tadpole condition (7) fixes

$$\Sigma_0 = ig_A ND \int \frac{dk}{2\pi} D_X(k) \tag{22}$$

so that

$$m^2 = m_0^2 + 2\tilde{\lambda}_A \int \frac{dk}{2\pi} D_X(k). \tag{23}$$

At leading order for large D we have $D_X(k) = 1/(k^2 + m^2)$ so that

$$m^2 = m_0^2 + \tilde{\lambda}_A/m + \mathcal{O}(1/D). \tag{24}$$

It is useful to think of the bare mass as a function of m by writing

$$m_0^2 = m^2 - \tilde{\lambda}_A/m + \mathcal{O}(1/D). \tag{25}$$

Neglecting $\mathcal{O}(1/D)$ corrections, the entire range $-\infty < m_0^2 < \infty$ corresponds to $m^2 > 0$, so we always have a positive dressed mass even if the bare fields are tachyonic. From (24) we see that $m^2 > m_0^2$ and from (20) we see that $m_\sigma^2 > 4m^2$.

It is the leading large-D behavior of the dressed mass that will be most relevant for us, especially in Sec. III. We denote this leading large-D behavior by m_1, with

$$m_1^2 = m_0^2 + \tilde{\lambda}_A/m_1. \tag{26}$$

Thus, m_1 agrees with m up to $\mathcal{O}(1/D)$ corrections.

C. Finite-temperature results

We now study the model at finite temperature, with the goal of understanding dissipation in the $1/D$ expansion. We do this using a Euclidean formalism, by discretizing the loop integrals to Matsubara sums,

$$\omega \to \omega_n = \frac{2\pi n}{\beta} \tag{27}$$

$$\int \frac{d\omega}{2\pi} \to \frac{1}{\beta}\sum_n. \tag{28}$$

We will repeat the steps in the previous section: first determine the σ propagator at leading order for large D, then determine the X^i propagator to $\mathcal{O}(1/D)$.

For σ this gives the leading-order propagator

$$D_\sigma^{-1}(\omega_n) = 1 + \tilde{\lambda}_A \frac{1}{\beta}\sum_n \frac{1}{k_n^2 + m^2}\frac{1}{(k_n + \omega_n)^2 + m^2}. \tag{29}$$

Following the standard Saclay technique [13–15] we switch to writing the propagators in position space,

$$\frac{1}{\omega^2 + m^2} = \int_0^\beta d\tau\, e^{i\omega\tau}\frac{1}{2m}[(1 + N_m)e^{-m\tau} + N_m e^{m\tau}] \tag{30}$$

where $N_m = \frac{1}{e^{\beta m} - 1}$ is a Bose distribution. Then we do the Matsubara sum using

$$\frac{1}{\beta}\sum_n e^{i2\pi n(\tau - \tau')/\beta} = \sum_w \delta(\tau - \tau' - \beta w). \tag{31}$$

The δ function kills one of the integrals over Euclidean time, and the remaining time integral leads to

$$D_\sigma^{-1}(\omega_n) = 1 + \frac{\tilde{\lambda}_A}{(2m)^2} N_m^2 \left[\frac{4m}{\omega_n^2 + 4m^2} (e^{2\beta m} - 1) + 2\beta e^{\beta m} \delta_{n,0} \right]. \tag{32}$$

The last term, proportional to $\delta_{n,0}$, comes from the cross terms between $e^{-m\tau}$ and $e^{+m\tau}$. We take the inverse to get the propagator itself. This gives a rather complicated expression which for convenience we write in the form

$$D_\sigma(\omega_n) = 1 - \frac{m_\sigma^2 - 4m^2}{\omega_n^2 + m_\sigma^2} - A\delta_{n,0}. \tag{33}$$

Here we have defined a thermally corrected σ mass

$$m_\sigma^2 = 4m^2 + \frac{\tilde{\lambda}_A}{m} \frac{e^{2\beta m} - 1}{(e^{\beta m} - 1)^2}. \tag{34}$$

We have also introduced a parameter A to obtain the correct propagator for the zero mode. It is fixed by requiring that (32) and (33) are consistent when $n = 0$,

$$[D_\sigma(\omega_{n=0}) \text{ from } (32)] = \frac{4m^2}{m_\sigma^2} - A. \tag{35}$$

The parameter A is a way of accounting for the $\delta_{n,0}$ term in (32). Note that the $\delta_{n,0}$ term makes a positive contribution to the right-hand side of (32), so it decreases the value of $D_\sigma(\omega_{n=0})$, which means that A is positive.

Next we evaluate the X^i propagator to $\mathcal{O}(1/D)$. In terms of Matsubara sums we have

$$D_X^{-1}(\omega) = \omega^2 + m^2 - 4\frac{\tilde{\lambda}_C}{D}\frac{1}{\beta}\sum_n \frac{1}{k_n^2 + m^2} + 2\frac{\tilde{\lambda}_A}{D}\frac{1}{\beta}\sum_n \frac{1}{(k_n + \omega)^2 + m^2} D_\sigma(k_n) - 4\frac{\tilde{\lambda}_C^2}{D}\frac{1}{\beta^2}\sum_{n_1,n_2} \frac{1}{k_{n_1}^2 + m^2}\frac{1}{k_{n_2}^2 + m^2} \times \frac{1}{(k_{n_1} + k_{n_2} + \omega)^2 + m^2}. \tag{36}$$

The advantage of writing the σ propagator in the form (33) is that the Matsubara sums are all straightforward, following the steps used to obtain (32). To $\mathcal{O}(1/D)$ we find

$$D_X^{-1}(\omega) = \omega^2 + m^2 + \frac{2\tilde{\lambda}_A - 4\tilde{\lambda}_C}{D} S_1 - \frac{2\tilde{\lambda}_A}{D}(m_\sigma^2 - 4m^2) S_2 - \frac{2\tilde{\lambda}_A}{D}\frac{A}{\beta}\frac{1}{\omega^2 + m^2} - \frac{4\tilde{\lambda}_C^2}{D} S_3 \tag{37}$$

where the sums (valid for Matsubara frequencies, $\omega \in \frac{2\pi}{\beta}\mathbb{Z}$) are[3]

$$S_1 = \frac{1}{\beta}\sum_n \frac{1}{k_n^2 + m^2} = \frac{1}{2m \tanh(\beta m/2)} \tag{38}$$

$$S_2 = \frac{1}{\beta}\sum_n \frac{1}{(k_n + \omega)^2 + m^2}\frac{1}{k_n^2 + m_\sigma^2} = \frac{N_m N_{m_\sigma}}{4 m m_\sigma}\left[(e^{\beta(m+m_\sigma)} - 1)\left(\frac{1}{i\omega + m_\sigma + m} - \frac{1}{i\omega - (m_\sigma + m)} \right) + (e^{\beta m_\sigma} - e^{\beta m})\left(\frac{1}{i\omega + m_\sigma - m} - \frac{1}{i\omega - (m_\sigma - m)} \right) \right] \tag{39}$$

$$S_3 = \frac{1}{\beta^2}\sum_{n_1,n_2} \frac{1}{k_{n_1}^2 + m^2}\frac{1}{k_{n_2}^2 + m^2}\frac{1}{(k_{n_1} + k_{n_2} + \omega)^2 + m^2} = \frac{N_m^3}{(2m)^3}\left[(e^{3\beta m} - 1)\left(\frac{1}{i\omega + 3m} - \frac{1}{i\omega - 3m} \right) + 3e^{\beta m}(e^{\beta m} - 1)\left(\frac{1}{i\omega + m} - \frac{1}{i\omega - m} \right) \right]. \tag{40}$$

Our goal is to study dissipation. To this end, since we are working in Euclidean space, we examine the behavior of the propagator in the vicinity of $\omega^2 + m^2 = 0$. Most of the loop corrections in (37) are small and make an $\mathcal{O}(1/D)$ shift in the location of the pole, but two terms (highlighted in magenta) are dangerous since they diverge at $\omega = \pm im$. Retaining just the dangerous terms we approximate the inverse propagator as

$$D_X^{-1}(\omega) = \omega^2 + m^2 - \frac{B}{\omega^2 + m^2} \tag{41}$$

[3]The expression for S_2 is valid provided $m \neq m_\sigma$, which is the case in our model. If one sets $m = m_\sigma$ in (39) there is an additional contribution to the sum proportional to $\delta_{n,0}$ that can be seen in (32).

where

$$B = \frac{2\tilde{\lambda}_A}{D}\frac{A}{\beta} + \frac{3\tilde{\lambda}_C^2}{Dm^2}N_m^2 e^{\beta m}. \tag{42}$$

In terms of the parameters of the model, the explicit expression for B that follows from (35) and (42) is

$$B = \frac{3\tilde{\lambda}_C^2}{4Dm^2\sinh^2\frac{\beta m}{2}} - \frac{2\tilde{\lambda}_A}{D\beta}\left[\frac{1}{1+\frac{\tilde{\lambda}_A}{4m^3}\left(\frac{1}{\tanh\frac{\beta m}{2}}+\frac{\beta m}{2\sinh^2\frac{\beta m}{2}}\right)} - \frac{1}{1+\frac{\tilde{\lambda}_A}{4m^3\tanh\frac{\beta m}{2}}}\right]. \tag{43}$$

Taking the inverse of (41), the propagator is

$$D_X(\omega) = \frac{1}{2}\left(\frac{1}{\omega^2+m^2+\sqrt{B}} + \frac{1}{\omega^2+m^2-\sqrt{B}}\right). \tag{44}$$

Recall that A is positive, which means that B is also positive. Also note that A is $\mathcal{O}(1)$ while B is $\mathcal{O}(1/D)$. So we see that at finite temperature the single pole at $\omega^2+m^2=0$ is split into a pair of nearby poles at $\omega^2+m^2\pm\sqrt{B}=0$.

To see the physical consequences we turn to the retarded Green's function $D_R(\omega)$, which can be obtained from a Euclidean correlator by analytically continuing [15,16][4]

$$D_R(\omega) = D_X(\omega_n \to -i(\omega+i\epsilon)). \tag{45}$$

This leads to

$$D_R(\omega) = \frac{1}{2}\left(\frac{1}{-(\omega+i\epsilon)^2+m_+^2} + \frac{1}{-(\omega+i\epsilon)^2+m_-^2}\right) \tag{46}$$

where

$$m_\pm^2 = m^2 \pm \sqrt{B}. \tag{47}$$

At finite temperature effectively there are two nearby energy levels. The consequences are clearest if we transform back to position space, where

$$\begin{aligned} D_R(t) &= \int \frac{d\omega}{2\pi} e^{-i\omega t} D_R(\omega) \\ &= \theta(t)\frac{1}{2}\left(\frac{1}{m_+}\sin(m_+ t) + \frac{1}{m_-}\sin(m_- t)\right) \\ &\approx \theta(t)\frac{1}{m}\sin(mt)\cos\left(\frac{\sqrt{B}t}{2m}\right). \end{aligned} \tag{48}$$

The model behaves as though it were a discrete quantum mechanical system. Although there is no true dissipation, the two nearby energy levels lead to destructive interference on a timescale given by

$$\tau = \frac{\pi m}{\sqrt{B}}. \tag{49}$$

We define an effective width for the excitation by

$$\Gamma = \frac{1}{\tau} = \frac{\sqrt{B}}{\pi m}. \tag{50}$$

This is exponentially suppressed at low temperatures, where

$$B \sim e^{-\beta m} \qquad \Gamma \sim e^{-\beta m/2}. \tag{51}$$

In contrast the width grows linearly at high temperatures, where

$$\Gamma = \frac{\sqrt{3}\tilde{\lambda}_C}{\pi m^3\sqrt{D}\beta} + \mathcal{O}(\beta). \tag{52}$$

Finally we examine thermal corrections to the relation between the parameter m and the bare parameters of the model (1). At finite temperature the tadpole condition (7) fixes

$$\Sigma_0 = ig_A N D\frac{1}{\beta}\sum_n D_X(k_n) \tag{53}$$

thus, from (5),

$$m^2 = m_0^2 + 2\tilde{\lambda}_A\frac{1}{\beta}\sum_n D_X(k_n). \tag{54}$$

At leading order for large D we have $D_X(k) = 1/(k^2+m^2)$ so that

$$m^2 = m_0^2 + \frac{\tilde{\lambda}_A}{m\tanh(\beta m/2)} + \mathcal{O}(1/D). \tag{55}$$

We can think of the bare mass as a function of m by writing

$$m_0^2 = m^2 - \frac{\tilde{\lambda}_A}{m\tanh(\beta m/2)} + \mathcal{O}(1/D). \tag{56}$$

[4]Our conventions for Wick rotating are $\omega_{\text{Minkowski}} = +i\omega_{\text{Euclidean}}$ and $t_{\text{Minkowski}} = -it_{\text{Euclidean}}$.

FIG. 4. Schwinger-Dyson equation in the leading order of $1/D$ expansion. In this leading order, only the snail diagrams contribute.

The entire range $-\infty < m_0^2 < \infty$ corresponds to $m^2 > 0$, so we always have a positive dressed mass even if the bare fields are tachyonic. This suggests there is no phase transition in the model.

III. DIRECT APPROACH

The same results can be obtained by directly analyzing the action (1).

A. Zero-temperature results

1. Leading order in $1/D$

The two-point function for X_{ij} field is

$$\langle X_{ij}(\tau)X_{kl}(0)\rangle = G(\tau)\delta_{il}\delta_{jk} \tag{57}$$

and its Fourier transformation is

$$G(\tau)=\int\frac{d\omega}{2\pi}G(\omega)e^{-i\omega\tau},\quad G(\omega)=\int d\tau G(\tau)e^{i\omega\tau}. \tag{58}$$

The bare propagator is $G_0(\omega)$, and the Schwinger-Dyson equation for the dressed propagator $G(\omega)$ in the leading order in $1/D$ expansion becomes

$$\begin{aligned} &G_0=\frac{1}{\omega^2+m_0^2},\quad G=\frac{1}{\omega^2+m_1^2},\\ &G(\omega)=G_0(\omega)-c_L\tilde{\lambda}_A G_0(\omega)G(\omega)\int\frac{d\omega'}{2\pi}G(\omega'). \end{aligned} \tag{59}$$

This is obtained from the snail Feynman diagrams shown in Fig. 4. Here, c_L is a constant determined by counting Wick contractions, and it turns out $c_L = 2$ (see Appendix C 1). The one-loop integral can be performed

$$\int d\omega' G(\omega') = \int d\omega' \frac{1}{\omega'^2 + m_1^2} = \frac{\pi}{m_1} \tag{60}$$

and thus,

$$G_0(\omega)^{-1} = G(\omega)^{-1} - \frac{\tilde{\lambda}_A}{m_1} \Rightarrow m_1^2 = m_0^2 + \frac{\tilde{\lambda}_A}{m_1}. \tag{61}$$

This matches with (26).

2. A bubble chain diagram for $1/D$ corrections

To evaluate $1/D$ corrections, we will have to take into account diagrams with a "bubble chain." The bubble chain Feynman diagrams are defined in Fig. 5. We denote them by $B(\omega)$, where $B(\omega)$ is the amplitude of the bubble chain diagrams such that there is a momentum flow $\omega = \omega_1 - \omega_2 \equiv \omega_{1-2}$.

From Fig. 5, in Euclidean signature $B(\omega)$ satisfies

$$\begin{aligned} B(\omega_{1-2}) = &\int\frac{d\omega}{2\pi}G(\omega)G(\omega_{1-2}-\omega)\\ &- c_B\lambda_A D\int\frac{d\omega}{2\pi}G(\omega)G(\omega_{1-2}-\omega)B(\omega_{1-2}). \end{aligned} \tag{62}$$

Here c_B is a coefficient. This shows that the bubble chain diagrams have a geometric sum structure as

$$B(\omega_{1-2}) = \frac{\int\frac{d\omega}{2\pi}G(\omega)G(\omega_{1-2}-\omega)}{1+c_B\tilde{\lambda}_A\int\frac{d\omega}{2\pi}G(\omega)G(\omega_{1-2}-\omega)}. \tag{63}$$

In Appendix C 2, we count Wick contractions and show that $c_B = 1$. One can compute the integral using

$$G(\tau) = \frac{1}{2m_1}(\theta(\tau)e^{-m_1\tau} + \theta(-\tau)e^{m_1\tau}) \tag{64}$$

as

$$\begin{aligned} &\int\frac{d\omega}{2\pi}G(\omega)G(\omega_{1-2}-\omega)\\ &=\int d\tau G(\tau)^2 e^{i\omega_{1-2}\tau}\\ &=\frac{1}{m_1}\int d\tau\frac{1}{4m_1}(\theta(\tau)e^{-2m_1\tau}+\theta(-\tau)e^{2m_1\tau})e^{i\omega_{1-2}\tau}\\ &=\frac{1}{m_1}\frac{1}{\omega_{1-2}^2+4m_1^2}. \end{aligned} \tag{65}$$

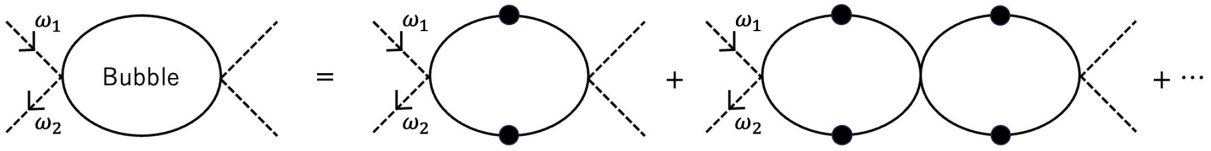

FIG. 5. Bubble chain diagram with a momentum flow $\omega_1 - \omega_2$. The black circle propagator represents $G(\omega)$ which we already obtained in (61).

From this, $B(\omega)$ can be determined as

$$B(\omega) = \frac{1}{m_1}\frac{1}{\omega^2 + m_\sigma^2}, \quad \text{where } m_\sigma^2 = 4m_1^2 + \frac{\tilde{\lambda}_A}{m_1}. \tag{66}$$

This expression for m_σ agrees with (20) up to $\mathcal{O}(1/D)$ corrections coming from the difference between m and m_1. Likewise the bubble chain propagator $B(\omega)$ is related to $D_\sigma(\omega)$ obtained in (19) as

$$1 - \tilde{\lambda}_A B(\omega) = 1 - \frac{\tilde{\lambda}_A}{m_1}\frac{1}{\omega^2 + m_\sigma^2} = 1 - \frac{m_\sigma^2 - 4m_1^2}{\omega^2 + m_\sigma^2} = D_\sigma(\omega) \tag{67}$$

again up to $\mathcal{O}(1/D)$ corrections coming from the difference between m and m_1. For $\tilde{\lambda}_A > 0$ note that $m_\sigma > 2m_1$. For future reference the Fourier transform of $B(\omega)$ is

$$B(\tau) = \frac{1}{2m_1 m_\sigma}(\theta(\tau)e^{-m_\sigma\tau} + \theta(-\tau)e^{m_\sigma\tau}). \tag{68}$$

3. $\tilde{\lambda}_A/D$ corrections for dissipation

Now we can evaluate the $1/D$ corrections to a two-point function which are responsible for dissipation. We will only be interested in diagrams that introduce ω dependence. There are additional self-energy diagrams that shift the mass; we ignore these diagrams for now and return to them in Sec. III A 5.

There are two types of $1/D$ corrections, one is proportional to $\tilde{\lambda}_A/D$ and the other is proportional to $\tilde{\lambda}_C/D$. We first consider only the contribution of $\tilde{\lambda}_A$. In other words, we set $\tilde{\lambda}_C = 0$ for a moment. Then the Feynman diagram proportional to $\tilde{\lambda}_A/D$ that contributes to dissipation, i.e., which produces a pole, is shown in Fig. 6.

Again we denote $G(\omega)$ as the leading dressed correlator in the large-D limit, i.e., the propagator without $1/D$ correction given by (59). Its mass m_1 is determined by (61) in the zero-temperature limit. We denote $\tilde{G}(\omega)$ as the dressed correlator including $1/D$ corrections. The Schwinger-Dyson equation taking into account $\tilde{\lambda}_A/D$ corrections becomes

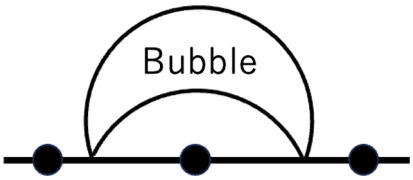

FIG. 6. The self-energy diagram proportional to $\tilde{\lambda}_A/D$ which contributes to dissipation. The black circle propagators are dressed propagators $G(\omega)$ which we already obtained in (61) and do not include any $1/D$ corrections. "Bubble" means the bubble chain diagram from Fig. 5. This diagram makes an ω-dependent contribution.

$$\tilde{G}(\omega)^{-1} = G(\omega)^{-1} - \frac{c_A\tilde{\lambda}_A^2}{D}\int\frac{d\omega_1}{2\pi}G(\omega_1)B(\omega-\omega_1) + \delta m_A + \mathcal{O}\left(\frac{1}{D^2}\right). \tag{69}$$

Here we are focusing on the self-energy correction shown in Fig. 6, since as we will see it has a pole. In addition δm_A represents the ω-independent $\mathcal{O}(\tilde{\lambda}_A/D)$ contributions coming from tadpole diagrams that are responsible for the $\mathcal{O}(\tilde{\lambda}_A/D)$ mass shift, i.e., they are parts of the mass difference $m - m_1$. c_A is a combinatoric constant that has the value $c_A = 2$, as shown in Appendix C 3.

Since

$$G(\tau)B(\tau) = \frac{m_1 + m_\sigma}{2m_1^2 m_\sigma}\frac{1}{2(m_1+m_\sigma)} \times (\theta(\tau)e^{-(m_1+m_\sigma)\tau} + \theta(-\tau)e^{(m_1+m_\sigma)\tau}) \tag{70}$$

we obtain

$$\int\frac{d\omega_1}{2\pi}G(\omega_1)B(\omega-\omega_1) = \int d\tau G(\tau)B(\tau)e^{i\omega\tau} = \frac{m_1+m_\sigma}{2m_1^2m_\sigma}\frac{1}{\omega^2+(m_1+m_\sigma)^2}. \tag{71}$$

Thus,

$$-\frac{2\tilde{\lambda}_A^2}{D}\int\frac{d\omega_1}{2\pi}G(\omega_1)B(\omega-\omega_1) = -\frac{\tilde{\lambda}_A^2}{D}\frac{m_1+m_\sigma}{m_1^2m_\sigma}\frac{1}{\omega^2+(m_1+m_\sigma)^2} \equiv \frac{1}{D}\Pi_A(\omega). \tag{72}$$

The fact that it has a pole at $m_1 + m_\sigma$ is important.

Thus, the Schwinger-Dyson equation becomes

$$\tilde{G}(\omega)^{-1} = \omega^2 + m_1^2 + \frac{1}{D}\Pi_A(\omega) + \delta m_A + \mathcal{O}\left(\frac{1}{D^2}\right) \tag{73}$$

where

$$\frac{1}{D}\Pi_A(\omega) = -\frac{\tilde{\lambda}_A}{D}\frac{\tilde{\lambda}_A}{m_1}\frac{m_1+m_\sigma}{m_1m_\sigma}\frac{1}{\omega^2+(m_1+m_\sigma)^2} \tag{74}$$

$$= \frac{\tilde{\lambda}_A}{D}\frac{1}{m_1m_\sigma}\frac{(4m_1^2-m_\sigma^2)(m_1+m_\sigma)}{\omega^2+(m_1+m_\sigma)^2}. \tag{75}$$

In the second equality, we use (66) that relates $\tilde{\lambda}_A$ by m_σ and m_1. This equation can be compared with $\tilde{\lambda}_A$ term in (21), where

$$\frac{\tilde{\lambda}_A}{mD}\frac{\omega^2+5m^2+mm_\sigma+4m^3/m_\sigma}{\omega^2+(m+m_\sigma)^2} = \frac{\tilde{\lambda}_A}{D}\frac{1}{mm_\sigma}\left(m_\sigma+\frac{(4m^2-m_\sigma^2)(m+m_\sigma)}{\omega^2+(m+m_\sigma)^2}\right). \quad (76)$$

Thus, the pole and its residue match completely. We also see certain $\mathcal{O}(1/D)$ contributions to the mass difference $m-m_1=\mathcal{O}(1/D)$.

4. $\tilde{\lambda}_C/D$ contributions for dissipation

For a complete computation of the $1/D$ correction to a two-point function, we must incorporate the effect of $\tilde{\lambda}_C=g_C^2ND$ as well. Then the Schwinger-Dyson equation becomes

$$\tilde{G}(\omega)^{-1}=\omega^2+m_1^2+\frac{1}{D}(\Pi_A(\omega)+\Pi_C(\omega)) + \delta m_A+\delta m_C+\mathcal{O}\left(\frac{1}{D^2}\right). \quad (77)$$

Here the melon diagram of Fig. 7 contributes to the self-energy as

$$\frac{1}{D}\Pi_C(\omega)=-\frac{c_C\tilde{\lambda}_C^2}{D}\int\frac{d\omega_1}{2\pi}\int\frac{d\omega_2}{2\pi}G(\omega_1) \times G(\omega_2)G(\omega-\omega_1-\omega_2) \quad (78)$$

$$=-\frac{c_C\tilde{\lambda}_C^2}{D}\int d\tau_1(G(\tau_1))^3e^{i\omega\tau_1} \quad (79)$$

$$=-\frac{3c_C\tilde{\lambda}_C^2}{4Dm_1^2}\frac{1}{\omega^2+9m_1^2} \quad (80)$$

where c_C is a combinatoric constant and $c_C=4$ which we show in Appendix C 4. Comparing to the term proportional to $\tilde{\lambda}_C/D$ in (21), we see that the pole and its residue match completely. We also see certain $\mathcal{O}(\tilde{\lambda}_C/D)$ contributions to the mass difference $m-m_1$.

Note that there is also a melon diagram proportional to $\tilde{\lambda}_A=g_A^2ND$. This melon diagram is obtained by replacing the bubble chain diagram in Fig. 6 by the first term on the right-hand side of Fig. 5. However, note that the results from the two melon diagrams are very different. The melon diagram in Fig. 7 proportional to $\tilde{\lambda}_C$ gives a pole at $\omega^2=-(3m_1)^2$. On the other hand, the melon diagram in Fig. 6 proportional to $\tilde{\lambda}_A$ gives a pole at $\omega^2=-(m_1+m_\sigma)^2$.

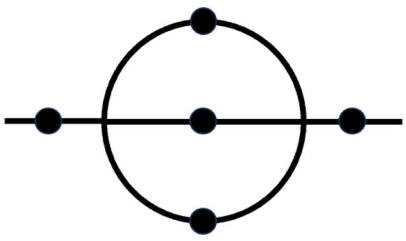

FIG. 7. Melon diagram which contributes in $\tilde{\lambda}_C/D$ corrections.

5. $1/D$ contributions to the mass shift

Recall that we have introduced two slightly different definitions of dressed mass. In Sec. II, m is defined by the no-tadpole condition which leads to (23). In Sec. III A 1 we defined a leading large-D dressed mass m_1 by solving a Schwinger-Dyson equation which leads to (26). The two definitions (23) and (26) differ by $\mathcal{O}(1/D)$ corrections.

In the direct approach of Sec. III, there are many diagrams that are responsible for $\mathcal{O}(1/D)$ corrections to the mass. We should take into account these $\mathcal{O}(1/D)$ mass shift corrections for comparison with the results in Sec. II.

For example, the snail diagrams in Fig. 4 make a subleading $\mathcal{O}(1/D)$ correction to the mass. It comes from the following Wick contraction:

$$+\frac{g_A^2}{2}\times 4\times\sum_{j,k=1}^{D}\overbrace{X^i(\overbrace{X^j\overbrace{X^k\overbrace{X^k}X^j}}^{}}^{}X^i) \quad (81)$$

which gives part of the $\mathcal{O}(1/D)$ mass shift, δm_A, in (73) [or in (77)] as

$$\delta m_A=\frac{2\tilde{\lambda}_A}{D}\int\frac{d\omega_1}{2\pi}G(\omega_1)+\cdots=\frac{\tilde{\lambda}_A}{Dm_1}+\cdots. \quad (82)$$

This mass shift can be compared with the ω-independent term in (21) or equivalently in (76).

Similarly, there is an additional mass shift contribution of $\mathcal{O}(\tilde{\lambda}_C/D)$, which is the snail diagram in Fig. 4 but it is obtained by the λ_C term where all indices are the same. More explicitly,

$$-\frac{g_C^2}{2}\times 4\times 2\times\sum_{j=1}^{D}\overbrace{X^i(\overbrace{X^j\overbrace{X^j\overbrace{X^j}X^j}}^{}}^{}X^i) \quad (83)$$

where 4 is because of four X^j's and 2 is because of two choices for $\overbrace{X^jX^j}$. The self-energy from such a diagram gives

$$\delta m_C=-\frac{4\tilde{\lambda}_C}{D}\int\frac{d\omega}{2\pi}G(\omega)+\cdots=-\frac{4\tilde{\lambda}_C}{2m_1D}+\cdots. \quad (84)$$

Again this mass shift can be compared with the ω-independent term in (21).

In addition to these $\mathcal{O}(1/D)$ snail diagrams, many other diagrams are responsible for the mass shift. Examples of such diagrams are shown in Fig. 8. Since our main interests are in dissipation in many-matrix models, we will not evaluate these mass shift contributions any further.

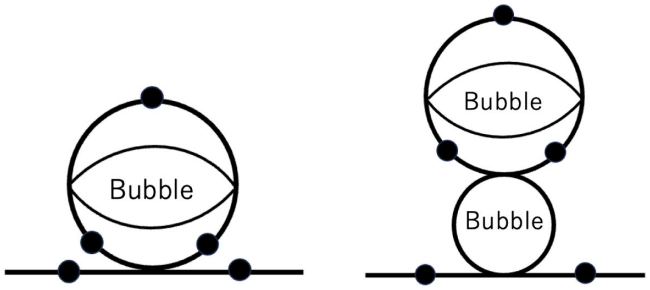

FIG. 8. Examples of diagrams which contribute to the mass shift at order $\tilde{\lambda}_A/D$. These tadpole diagrams are ω independent. They contribute to the mass shift at $\mathcal{O}(1/D)$.

B. Finite-temperature results

1. Leading order in $1/D$

At finite temperature, momentum is discretized as in (27) by Matsubara frequency and the integral becomes summation as in (28). The Schwinger-Dyson equation in the leading order in $1/D$ becomes

$$G(\omega_n) = G_0(\omega_n) - c_L \frac{\tilde{\lambda}_A}{\beta} G_0(\omega_n) G(\omega_n) \sum_k G(\omega_k) \tag{85}$$

with $c_L = 2$. This becomes

$$m_1^2 = m_0^2 + \frac{\tilde{\lambda}_A}{m_1} \coth \frac{\beta m_1}{2}. \tag{86}$$

In zero-temperature limit $m_1\beta \gg 1$, this becomes

$$m_1^2 = m_0^2 + \frac{\tilde{\lambda}_A}{m_1} \tag{87}$$

which matches with (26).

On the other hand, in high temperature limit $m_1\beta \ll 1$, this becomes

$$m_1^2 \sim \frac{\tilde{\lambda}_A}{m_1} \frac{2}{\beta m_1} = \frac{2\tilde{\lambda}_A}{\beta m_1^2}. \tag{88}$$

2. A bubble chain diagram for $1/D$ corrections

Let us perform a similar analysis for nonzero temperature. The analysis becomes complicated, but physically, the effective mass changes in finite temperature. First, let us see the bubble chain diagram for nonzero temperature. We can rewrite the Schwinger-Dyson equation as one with finite temperature,

$$\begin{aligned} B((\omega_{1-2})_n) = {} & \frac{1}{\beta} \sum_k G(\omega_k) G((\omega_{1-2})_n - \omega_k) \\ & - \frac{c_B \lambda_A D}{\beta} \sum_k G(\omega_k) G((\omega_{1-2})_n - \omega_k) \\ & \times B((\omega_{1-2})_n). \end{aligned} \tag{89}$$

Again, $c_B = 1$ and this yields

$$B((\omega_{1-2})_n) = \frac{\frac{1}{\beta}\sum_k G(\omega_k) G((\omega_{1-2})_n - \omega_k)}{1 + \frac{c_B \lambda_A D}{\beta} \sum_k G(\omega_k) G((\omega_{1-2})_n - \omega_k)}. \tag{90}$$

This summation can be computed as follows:

$$\frac{1}{\beta} \sum_k G(\omega_k) G(\omega_n - \omega_k) = \frac{1}{m_1} \frac{\coth \frac{m_1\beta}{2}}{\omega_n^2 + 4m_1^2} + \frac{\beta \operatorname{csch}^2 \frac{m_1\beta}{2}}{8m_1^2} \delta_{n,0}. \tag{91}$$

Therefore, separated contributions due to zero mode appear in a bubble chain diagram as well. We can simply write them as follows:

$$B(\omega_n) = \frac{1}{m_1} \frac{\coth \frac{m_1\beta}{2}}{\omega_n^2 + m_\sigma^2} + \frac{A}{\tilde{\lambda}_A} \delta_{n,0} \tag{92}$$

where m_σ is β-dependent mass,

$$m_\sigma^2 = 4m_1^2 + \frac{\tilde{\lambda}_A}{m_1} \coth \frac{m_1\beta}{2}, \tag{93}$$

and A is a complicated β-dependent function,

$$\frac{A}{\tilde{\lambda}_A} = \frac{4\beta m_1^4}{(4m_1^3 + \tilde{\lambda}_A \coth(\frac{\beta m_1}{2}))(4m_1^3(\cosh(\beta m_1) - 1) + \tilde{\lambda}_A(\beta m_1 + \sinh(\beta m_1)))}. \tag{94}$$

Note that A is positive since $\tilde{\lambda}_A > 0$.

Since $\lim_{\beta\to\infty} A(\beta) \to 0$,

$$m_\sigma^2 \to 4m_1^2 + \frac{\tilde{\lambda}_A}{m_1}, \qquad B(\omega_n) \to \frac{1}{m_1} \frac{1}{\omega_n^2 + 4m_1^2 + \frac{\tilde{\lambda}_A}{m_1}}, \quad \text{as } m_1\beta \to \infty. \tag{95}$$

Note also that $m_\sigma > 2$ at any temperature as long as the theory is not free, i.e., $\tilde{\lambda}_A > 0$.

We also have

$$1-\tilde{\lambda}_A B(\omega_n) = 1-\frac{\tilde{\lambda}_A}{m_1}\frac{\coth\frac{m_1\beta}{2}}{\omega_n^2+m_\sigma^2} - A\delta_{n,0} = 1-\frac{m_\sigma^2-4m_1^2}{\omega_n^2+m_\sigma^2} - A\delta_{n,0} = D_\sigma(\omega_n) \quad (96)$$

which matches with $D_\sigma(\omega_n)$ in (33) up to $\mathcal{O}(1/D)$ corrections coming from the mass difference $m-m_1=\mathcal{O}(1/D)$.

3. $1/D$ corrections for dissipation

Similar to the zero-temperature case, the Schwinger-Dyson equation can be rewritten as

$$\tilde{G}(\omega_n)^{-1} = G(\omega_n)^{-1} + \frac{1}{D}(\Pi_A(\omega_n)+\Pi_C(\omega_n)) + \delta m_A + \delta m_C + O\left(\frac{1}{D^2}\right) \quad (97)$$

$$\frac{1}{D}\Pi_A(\omega_n) = -\frac{c_A}{D}\frac{\tilde{\lambda}_A^2}{\beta}\sum_k G(\omega_k)B(\omega_k-\omega_n) \quad (98)$$

$$\frac{1}{D}\Pi_C(\omega_n) = -\frac{c_C}{D}\frac{\tilde{\lambda}_C^2}{\beta^2}\sum_{k,k'} G(\omega_k)G(\omega_{k'})G(\omega_n-\omega_{k+k'}) \quad (99)$$

where $c_A=2$, $c_C=4$. Π_A and Π_C contributions are given by Figs. 6 and 7, respectively.

Contribution for Π_A yields

$$\frac{1}{D}\Pi_A(\omega_n) = -\frac{c_A}{D}\frac{\tilde{\lambda}_A^2}{\beta}\sum_k G(\omega_k)B(\omega_n-\omega_k) = -\frac{c_A}{D}\tilde{\lambda}_A^2\coth\frac{m_1\beta}{2}\frac{m_\sigma\coth(\frac{Bm_1}{2})(-m_1^2+m_\sigma^2+\omega_n^2)+m_1\coth(\frac{Bm_\sigma}{2})(m_1^2-m_\sigma^2+\omega_n^2)}{2m_1^2m_\sigma((m_1-m_\sigma)^2+\omega_n^2)((m_1+m_\sigma)^2+\omega_n^2)} - \frac{B_1}{\omega_n^2+m_1^2}, \quad (100)$$

where $c_A=2$ and

$$B_1 = \frac{2}{D}\frac{\tilde{\lambda}_A}{\beta}A. \quad (101)$$

Contribution for Π_C yields

$$\begin{aligned}\frac{1}{D}\Pi_C(\omega_n) &= -\frac{c_C}{D}\frac{\tilde{\lambda}_C^2}{\beta^2}\sum_{k,k'} G(\omega_k)G(\omega_{k'})G(\omega_n-\omega_{k+k'}) \\ &= -\frac{c_C}{D}\frac{\tilde{\lambda}_C^2}{\beta}\sum_k G(\omega_k)\left(\frac{1}{\beta}\sum_{k'} G(\omega_{k'})G(\omega_n-\omega_{k+k'})\right) \\ &= -\frac{c_C}{D}\frac{\tilde{\lambda}_C^2}{\beta}\sum_k G(\omega_k)\left(\frac{1}{m_1}\frac{\coth\frac{m_1\beta}{2}}{\omega_{n-k}^2+4m_1^2}+\frac{\beta\,\mathrm{csch}^2\frac{m_1\beta}{2}}{8m_1^2}\delta_{n-k,0}\right) \\ &= -\frac{c_C}{D}\frac{\tilde{\lambda}_C^2}{16m_1^2}\left(\frac{\mathrm{csch}^2\frac{m_1\beta}{2}}{\omega_n^2+m_1^2}+\frac{3(4+3\mathrm{csch}^2\frac{m_1\beta}{2})}{\omega_n^2+9m_1^2}\right) - \frac{c_C}{D}\frac{\tilde{\lambda}_C^2}{8m_1^2}\mathrm{csch}^2\frac{m_1\beta}{2}G(\omega_n) \\ &= -\frac{B_2}{\omega_n^2+m_1^2} - \frac{3c_C\tilde{\lambda}_C^2}{16Dm_1^2}\frac{4+3\mathrm{csch}^2\frac{m_1\beta}{2}}{\omega_n^2+9m_1^2}\end{aligned} \quad (102)$$

where $c_C=4$ and

$$B_2 = \frac{3c_C\tilde{\lambda}_C^2}{16Dm_1^2}\mathrm{csch}^2\frac{m_1\beta}{2} = \frac{3c_C\tilde{\lambda}_C^2}{4Dm_1^2}\left(\frac{1}{e^{\beta m_1}-1}\right)^2 e^{\beta m_1}. \quad (103)$$

Combining (103) with (101), we obtain the propagator in the vicinity of $\omega^2+m_1^2=0$ as

$$\tilde{G}(\omega_n)^{-1} = G(\omega_n)^{-1} + \frac{1}{D}(\Pi_A(\omega_n) + \Pi_C(\omega_n)) + \delta m_A + \delta m_C + O\left(\frac{1}{D^2}\right) \tag{104}$$

where

$$\frac{1}{D}(\Pi_A(\omega_n) + \Pi_C(\omega_n)) = -\frac{B}{\omega_n^2 + m_1^2} + \cdots, \tag{105}$$

$$B = B_1 + B_2 = \frac{1}{D}\left(\frac{2\tilde{\lambda}_A A}{\beta} + \frac{3\tilde{\lambda}_C^2}{m_1^2}\left(\frac{1}{e^{\beta m_1} - 1}\right)^2 e^{\beta m_1}\right). \tag{106}$$

This matches the previous results (41) and (42), neglecting the additional $\mathcal{O}(1/D)$ corrections coming from the mass difference $m - m_1 = \mathcal{O}(1/D)$. Thus, the rest of the argument that, at finite temperature, the single pole at $\omega^2 + m_1^2 = 0$ splits into a pair of nearby poles is the same as Sec. II.

IV. CONCLUSIONS

We studied a simple model of many-matrix quantum mechanics. From the matrix point of view we worked in the planar limit, sending $N \to \infty$ first. Physical quantities can then be calculated as an expansion in $1/D$, where D is the number of matrices. This can be thought of as a particular scaling limit of a tensor model. It can also be thought of as a noncommutative generalization of an $O(D)$ vector model.

We focused on dissipation at finite temperature, which we extracted from a two-point correlator. A curious fact is that dissipation arises at $\mathcal{O}(1/\sqrt{D})$. We expect that this is generically true in many-matrix models. Another curious fact is that at high temperature the leading dissipative effects are due to the coupling g_C, while g_A only makes subleading contributions. If we set $g_C = 0$ and then expand the width (50) for high temperatures, then unlike the linear growth (52) we find that the leading behavior is temperature independent,

$$\Gamma|_{\tilde{\lambda}_C = 0} = \frac{\sqrt{2}m}{\pi\sqrt{D}} + \mathcal{O}(\beta). \tag{107}$$

It would be interesting to understand why the couplings g_C and g_A lead to such different behaviors. As a possible explanation, note that for any N and D the potential of the model (1) can be written as

$$V = \frac{1}{2}m_0^2 \mathrm{Tr}(X^i X^i) - \frac{1}{4}g_C^2 \mathrm{Tr}([X^i, X^j]^2) + \frac{1}{2}(g_A^2 - g_C^2)\mathrm{Tr}(X^i X^i X^j X^j). \tag{108}$$

The mass term dominates near the origin. The (commutator)^2 term is stable, but has flat directions corresponding to commuting matrices. The last term is stable if $g_A > g_C$, but if $g_A < g_C$ it makes the potential unstable at large fields. Thus we see that

(i) For $g_A > g_C$ the model is stable.
(ii) For $g_A = g_C$ the quartic potential has flat directions. The model is stable for $m_0^2 \geq 0$.[5]
(iii) For $g_A < g_C$ the model has an instability at large fields.

This behavior appears to be independent of N and D. The instability for $g_A < g_C$ may be related to the different behaviors of the two couplings.[6]

It would also be interesting to explore higher orders in perturbation theory.

(i) To $\mathcal{O}(1/D)$, in the retarded propagator (45), we have seen that the pole at $\omega^2 = m^2$ that is present at tree level splits into a pair of poles at $\omega^2 = m_\pm^2$. Presumably at higher orders in $1/D$ the splitting continues and additional poles develop. Does the width Γ remain $\mathcal{O}(1/\sqrt{D})$?
(ii) At $\mathcal{O}(1/D)$ the correlator (48) undergoes a "recurrence" when $t = 4\pi m/\sqrt{B}$. As additional poles develop, does the recurrence timescale get longer?
(iii) Perhaps one can study the large-order behavior of perturbation theory. Does the model develop a continuous spectrum? Is there a sign of the instability which is present when $g_C > g_A$? Is the $1/D$ expansion convergent, or can it be resummed?

Another interesting direction is to add a massive vector as a probe [17,18]. It is known that, for a single free matrix coupled to a vector, the out-of-time-ordered correlators (OTOCs) for the vector do not grow exponentially in time [19,20]. This is because the matrix is free. For the interacting many-matrix model we studied in this paper, the matrices themselves have nontrivial dissipation. Thus, OTOCs for a vector coupled to our interacting matrices might show nontrivial behavior. It would be interesting to investigate this direction further.

ACKNOWLEDGMENTS

We are grateful to Matt Lippert, V. P. Nair, Rob Pisarski and Daniel Robbins for valuable discussions. The work of T. A. and N. I. were supported in part by JSPS KAKENHI Grants No. 24K22886(TA) and No. 18K03619(NI). The work of N. I. was also supported by MEXT KAKENHI Grant-in-Aid for Transformative Research Areas A "Extreme Universe" No. 21H05184. D. K. is supported by U.S. National Science Foundation Grant No. PHY-2112548.

[5]At large N and large D, (25) shows that the model is stable even for $m_0^2 < 0$. It would be interesting to explore this further and determine the conditions for stability when $m_0^2 < 0$.
[6]We thank V. P. Nair for suggesting this possibility.

DATA AVAILABILITY

No data were created or analyzed in this study.

APPENDIX A: AUXILIARY FIELDS

We briefly review the introduction of the auxiliary field Σ via a Hubbard-Stratonovich transformation [21]. Consider the 1D integral

$$Z = \int_{-\infty}^{\infty} d\phi e^{-S_E} \qquad S_E = \frac{1}{2}m^2\phi^2 + \frac{1}{2}g^2\phi^4. \tag{A1}$$

Introduce 1 in the path integral, represented as

$$1 = \frac{1}{\sqrt{2\pi}} \int_{-\infty}^{\infty} d\Sigma e^{-\frac{1}{2}(\Sigma - ig\phi^2)^2}. \tag{A2}$$

Up to a normalization this leads to

$$Z = \int d\phi d\Sigma e^{-S_E} \quad S_E = \frac{1}{2}m^2\phi^2 + \frac{1}{2}\Sigma^2 - ig\Sigma\phi^2. \tag{A3}$$

This action is analogous to (4). Note that in this form both ϕ and Σ are integrated over real values. In the literature one sometimes redefines Σ to absorb a factor of i.

APPENDIX B: COMBINATORICS FOR HUBBARD-STRATONOVICH APPROACH

In this appendix we fix the numerical factors that appear in the diagrams of Fig. 2, including the flipped forms mentioned in the caption. These factors are displayed in (16). The strategy is simple: We invert (16) and expand in powers of the couplings. Numerical factors are fixed by matching to ordinary perturbation theory.

In perturbation theory the two-point function is (with no sum on i, and with integrals over Euclidean time suppressed)

$$\langle X^i X^i e^{-S_{\rm int}} \rangle. \tag{B1}$$

The first diagram in Fig. 2, including its flipped form, comes from

$$\frac{1}{2} g_C^2 \langle X^i \mathrm{Tr}(X^j X^k X^j X^k) X^i \rangle. \tag{B2}$$

Restricting to planar diagrams there are four possible contractions for the X^i on the left, and two possible contractions for the X^i on the right. There is one closed matrix index loop, so the diagram comes with a numerical factor

$$\frac{1}{2} g_C^2 \cdot 4 \cdot 2 \cdot N = 4 g_C^2 N. \tag{B3}$$

The second diagram in Fig. 2, including its flipped form, arises at second order in perturbation theory. It comes from

$$\frac{1}{2!} (i g_A)^2 \langle X^i \mathrm{Tr}(\sigma X^j X^j) \mathrm{Tr}(\sigma X^k X^k) X^i \rangle. \tag{B4}$$

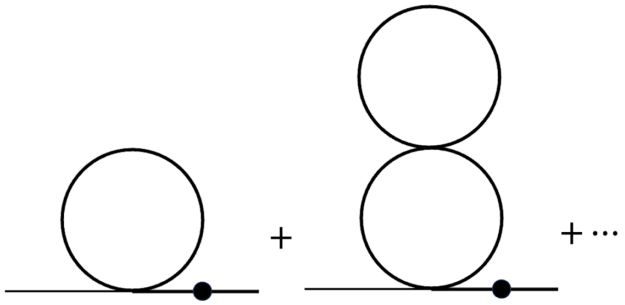

FIG. 9. Perturbative snail diagrams to two loops.

Again restricting to planar diagrams, there are two ways to contract the X fields in which the σ contraction runs below an X contraction. There are also two ways to contract the X fields in which the σ contraction runs above an X contraction. This gives a total of four possible contractions. There is one closed matrix index loop, so the diagram comes with a numerical factor

$$\frac{1}{2!} (i g_A)^2 \cdot 4 \cdot N = -2 g_A^2 N. \tag{B5}$$

The third diagram in Fig. 2 arises at second order in perturbation theory. It comes from

$$\frac{1}{2!} \left(\frac{1}{2} g_C^2 \right)^2 \langle X^i \mathrm{Tr}(X^j X^k X^j X^k) \mathrm{Tr}(X^m X^n X^m X^n) X^i \rangle. \tag{B6}$$

For a planar diagram there are eight possible contractions for the X^i on the left, followed by four possible contractions for the X^i on the right. There are two closed matrix index loops and one closed vector index loop, so the numerical factor is

$$\frac{1}{2!} \left(\frac{1}{2} g_C^2 \right)^2 \cdot 8 \cdot 4 \cdot N^2 \cdot D = 4 g_C^4 N^2 D. \tag{B7}$$

The numerical factors (B3), (B5), and (B7) appear inside the square brackets in (16).

APPENDIX C: COMBINATORICS FOR DIRECT APPROACH

In this appendix, we will calculate various combinatoric coefficients in various diagrams.[7]

1. Coefficient $c_L = 2$

This coefficient can be obtained by Wick contraction as follows. In perturbation theory, the snail diagrams are shown in Fig. 9 through two loops. The one-loop diagram in Fig. 9 is

[7]In this appendix, we use $a, b, c = 1, \cdots D$ for flavor indices and $i, j, k = 1, \cdots N$ for color indices.

$$X^a_{ij}\left(-\frac{g_A^2}{2}\sum_{b,c}\mathrm{Tr}(X^bX^bX^cX^c)\right)X^a_{kl} \tag{C1}$$

where X^a represents an external line. Considering the Trace cyclic property, the possible Wick contractions are as follows:

$$\begin{aligned}&-\frac{g_A^2}{2}\times 4\times\sum_{b,c=1}^{D}\overbrace{X^a_{ij}X^b_{mn}}X^b_{no}X^c_{op}X^c_{pm}X^a_{kl}\to-\frac{g_A^2}{2}\times 4\times\sum_{b,c=1}^{D}\overbrace{X^a_{ij}X^b_{mn}}\overbrace{X^b_{no}X^c_{op}X^c_{pm}}X^a_{kl}\\&=-2g_A^2\sum_{b,c=1}^{D}\delta^{ab}\delta^{cc}\delta_{in}\delta_{jm}\delta_{nl}\delta_{ok}\delta_{om}\delta_{pp}=-2\tilde{\lambda}_A\delta_{il}\delta_{jk}\end{aligned} \tag{C2}$$

Here "→" means we maintain only the leading contributions and neglect all subleading contributions. The number 4 is because there are four X's in $X^bX^bX^cX^c$. This determines

$$c_L=2. \tag{C3}$$

To simplify the notation, let us write only the subscripts of the matrix, such as $a\equiv X^a$. Then the two-loop diagram in Fig. 9 is

$$\frac{1}{2!}\left(-\frac{g_A^2}{2}\right)^2\sum_{b,c,d,e}X^a(X^bX^bX^cX^c)(X^dX^dX^eX^e)X^a=\frac{1}{2!}\left(-\frac{g_A^2}{2}\right)^2\sum_{b,c,d,e}a(bbcc)(ddee)a \tag{C4}$$

$$=\frac{(-g_A^2)^2}{2^3}\times 8\times\sum_{c,d,e}\overbrace{a(}aacc)(ddee)a\to\frac{(-g_A^2)^2}{2^3}\times 8\times\sum_{c,d,e}\overbrace{a(}\overbrace{aacc)}(ddee)a \tag{C5}$$

$$\to\frac{(-g_A^2)^2}{2^3}\times 8\times 2\times\sum_{c,d}\overbrace{a(}\overbrace{aa\overbrace{cc)(dd}cc)}a+\frac{(-g_A^2)^2}{2^3}\times 8\times 2\times\sum_{c,d}\overbrace{a(}\overbrace{aacc)(ddcc)}a \tag{C6}$$

where 8 is because there are eight X's in $bbccddee$ and 2 is because there are two choices d and e to pair up with c. The last term is also planar due to the trace cyclicity. Thus, in this two-loop diagram, the final coefficient is $(-2\lambda_A D)^2$. This also justifies (C3).

2. Coefficient $c_B=1$ in the bubble chain diagram

The coefficient c_B in a bubble diagram can be obtained similarly. First, we will calculate the coefficients in the perturbative bubble diagram as in Fig. 10.

The first term on the right-hand side of Fig. 10 is

$$\frac{1}{2!}\left(-\frac{g_A^2}{2}\right)^2\sum_{a,b,c,d}X^IX^I(X^aX^aX^bX^b)(X^cX^cX^dX^d)X^FX^F \tag{C7}$$

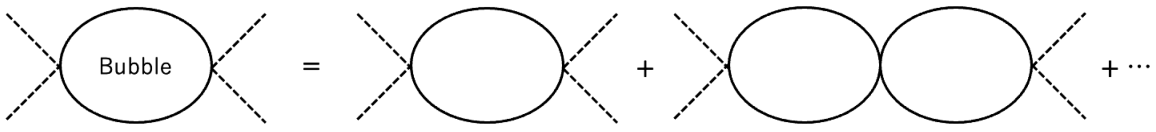

FIG. 10. Bubble chain diagrams.

and in the simplified notation, only the following Wick contraction needs to be considered if we distinguish between two external lines I's and the others F's:

$$\frac{(-g_A^2)^2}{2^3}\times 8\times 4\times \overbrace{II(\overbrace{aabb})(ccd\overbrace{d})FF} \tag{C8}$$

where 8 is because there are eight X's in $aabbccdd$, and 4 is to choose one in $ccdd$.

Then there are two choices to contract between b and c's,

$$\frac{(-g_A^2)^2}{2^3}\times 8\times 4\times \overbrace{II(\overbrace{aabb})(\overbrace{ccdd})FF} \tag{C9}$$

$$\frac{(-g_A^2)^2}{2^3}\times 8\times 4\times \overbrace{II(\overbrace{aabb})(\overbrace{ccdd})FF}. \tag{C10}$$

The first one is a planar diagram,

$$\begin{aligned}&\overbrace{I_{ij}\overbrace{I_{i'j'}(\overbrace{a_{mn}a_{no}}\overbrace{b_{op}\overbrace{b_{pm}})(\overbrace{c_{qr}c_{rs}}\overbrace{d_{st}\overbrace{d_{tq}})F_{kl}F_{k'l'}}}}}}\\&=\sum_{m,n,o,p,q,r,s,t}\delta_{io}\delta_{jn}\cdot\delta_{i'n}\delta_{j'm}\cdot\delta_{os}\delta_{pr}\cdot\delta_{pr}\delta_{mq}\cdot\delta_{sl'}\delta_{tk'}\cdot\delta_{tl}\delta_{qk}=N\delta_{il'}\delta_{ji'}\delta_{j'k}\delta_{lk'}\end{aligned} \tag{C11}$$

but the second one is nonplanar suppressed by $1/N$,

$$\overbrace{I_{ij}\overbrace{I_{i'j'}(\overbrace{a_{mn}a_{no}}\overbrace{b_{op}\overbrace{b_{pm}})(\overbrace{c_{qr}c_{rs}}\overbrace{d_{st}\overbrace{d_{tq}})F_{kl}F_{k'l'}}}}} \tag{C12}$$

$$=\sum_{m,n,o,p,q,r,s,t}\delta_{io}\delta_{jn}\cdot\delta_{i'n}\delta_{j'm}\cdot\delta_{or}\delta_{pq}\cdot\delta_{ps}\delta_{mr}\cdot\delta_{sl'}\delta_{tk'}\cdot\delta_{tl}\delta_{qk}=\delta_{ij'}\delta_{ji'}\delta_{lk'}\delta_{kl'}. \tag{C13}$$

Thus, the leading coefficient is

$$\frac{(-g_A^2)^2N}{2^3}\times 8\times 4=4\times\frac{(-\lambda_A D)^2}{ND}. \tag{C14}$$

The second term on the right-hand side of Fig. 10 is

$$\frac{1}{3!}\left(-\frac{g_A^2}{2}\right)^3\sum_{a,b,c,d,e,g}II(aabb)(ccdd)(eegg)FF. \tag{C15}$$

The contractions of I and F, respectively, can be written as follows:

$$12\cdot 8\cdot \overbrace{II(\overbrace{aabb})(ccdd)(ee\overbrace{gg})FF} \tag{C16}$$

where 12 is because of 12X's in $aabbccddeegg$ and 8 is because of eight X's in $ccddeegg$.

And there are four ways to contract,

$$12\cdot 8\cdot 2\cdot \overbrace{II(\overbrace{aabb})(\overbrace{ccdd})(\overbrace{eegg})FF} \tag{C17}$$

$$12\cdot 8\cdot 2\cdot \overbrace{II(\overbrace{aabb})(\overbrace{ccdd})(\overbrace{eegg})FF} \tag{C18}$$

$$12\cdot 8\cdot 2\cdot \overbrace{II(\overbrace{aabb})(\overbrace{ccdd})(\overbrace{eegg})FF} \tag{C19}$$

$$12\cdot 8\cdot 2\cdot \overbrace{II(\overbrace{aabb})(\overbrace{ccdd})(\overbrace{eegg})FF} \tag{C20}$$

where 2 is because of two choices between c and d. However, one can check that only (C17) is a planar,

$$\overbrace{I_{ij}\overbrace{I_{i'j'}(\overbrace{a_{mn}a_{no}}\overbrace{b_{op}\overbrace{b_{pm}})(\overbrace{c_{qr}c_{rs}}\overbrace{d_{st}\overbrace{d_{tq}})(\overbrace{e_{uv}e_{vw}}\overbrace{g_{wx}\overbrace{g_{xu}})F_{kl}F_{k'l'}}}}}} \tag{C21}$$

$$= \sum_{m,n,o,p,q,r,s,t,u,v,w,x} \delta_{io}\delta_{jn}\cdot\delta_{i'n}\delta_{j'm}\cdot\delta_{os}\delta_{pr}\cdot\delta_{pr}\delta_{mq}\cdot\delta_{sw}\delta_{tv}\cdot\delta_{tv}\delta_{qu}\cdot\delta_{wl'}\delta_{xk'}\cdot\delta_{xl}\delta_{uk} \tag{C22}$$

$$= N^2\delta_{il'}\delta_{ji'}\delta_{j'k}\delta_{lk'} \tag{C23}$$

and the rest are nonplanar. Thus, the leading coefficient is

$$\frac{1}{3!}\left(-\frac{g_A^2}{2}\right)^3 \times 12 \times 8 \times 2 = 4 \times \frac{(-\lambda_A D)^3}{ND}. \tag{C24}$$

Comparison between (C14) and (C24) gives

$$c_B = 1 \tag{C25}$$

for the bubble chain contribution given by the geometry sum as (63).

3. Coefficient $c_A = 2$ for Fig. 6

We would like to consider the contribution from resumed bubbles as in Fig. 6. For that purpose, let us first consider those with just one loop or two loops as in Figs. 11 and 12.

Let us consider Fig. 11 first. This is obtained from the term

$$\frac{1}{2!}\left(-\frac{g_A^2}{2}\right)^2 \sum_{b,c,d,e} a(bbcc)(ddee)a \tag{C26}$$

by the following Wick contractions:

$$4 \times 2 \times \frac{(-g_A^2)^2}{2^3} \sum_{b,c,d,e} \overbrace{a(bbcc)a(deed)} \quad \text{or} \quad 4 \times 2 \times \frac{(-g_A^2)^2}{2^3} \sum_{b,c,d,e} \overbrace{a(bccb)(deed)a} \tag{C27}$$

where 4 is for four choices in $bcde$ and 2 is for two choices in de, and the rest of the contractions are subleading.

From these two, we obtain

$$4 \times 2 \times \frac{(-g_A^2)^2}{2^3} \times 2 \times N^2 D = 2\frac{(-\lambda_A D)^2}{D}. \tag{C28}$$

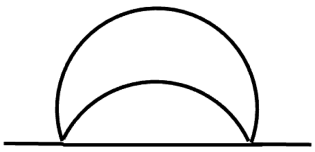

FIG. 11. One-loop bubble diagram, proportional to $2(-\lambda_A D)^2 \frac{1}{D}$.

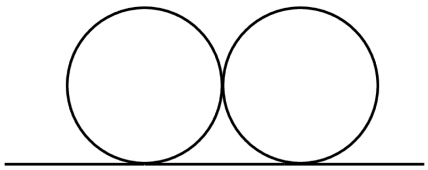

FIG. 12. Two-loop bubble diagram, proportional to $2(-\lambda_A D)^3 \frac{1}{D}$.

Next, let us consider Fig. 12,

$$\frac{1}{3!}\left(-\frac{g_A^2}{2}\right)^3 \sum_{b,c,d,e,f,g} a(bbcc)(ddee)(ffgg)a. \tag{C29}$$

We have the following Wick contractions in the leading order:

$$6 \times 4 \times 2 \times \frac{1}{3!}\left(-\frac{g_A^2}{2}\right)^3 \sum_{b,c,d,e,f,g} \overbrace{a(bbcc)(ddee)(ffgg)a} \tag{C30}$$

$$\text{or} \quad 6 \times 4 \times 2 \times \frac{1}{3!}\left(-\frac{g_A^2}{2}\right)^3 \sum_{b,c,d,e,f,g} \overbrace{a(bccb)(gffg)a(eedd)} \tag{C31}$$

where 6 is for six choices in $bcdefg$, 4 is for four choices in $defg$, and 2 is for two choices in de. Therefore, the coefficient is determined as

$$6\times4\times2\times\frac{1}{3!}\left(-\frac{g_A^2}{2}\right)^3\times2\times N^3D^2=2\frac{(-\lambda_A D)^3}{D}. \tag{C32}$$

From the above, we see that the overall coefficients of both Figs. 11 and 12 is 2. Thus, we can write down these diagram contributions as

$$\frac{2}{D}(-\lambda_A D)^2 G_0(\omega)G(\omega)\int\frac{d\omega_1}{2\pi}G(\omega_1)\left[\int\frac{d\omega'}{2\pi}G(\omega')G(\omega'-\omega+\omega_1)\right.$$
$$\left.+c_B(-\lambda_A D)\int\frac{d\omega'}{2\pi}G(\omega')G(\omega'-\omega+\omega_1)\int\frac{d\omega''}{2\pi}G(\omega'')G(\omega''-\omega+\omega_1)+\cdots\right]$$
$$=\frac{2}{D}(-\lambda_A D)^2 G_0(\omega)G(\omega)\int\frac{d\omega_1}{2\pi}G(\omega_1)B(\omega-\omega_1) \tag{C33}$$

with

$$c_A = 2. \tag{C34}$$

4. Coefficient $c_C = 4$

Let us consider the melon diagram, which plays an important role in the two-point function. From Fig. 13, this can be obtained from

$$\frac{1}{2!}\left(\frac{g_C^2}{2}\right)^2\sum_{b,c,d,e}a(bcbc)(dede)a. \tag{C35}$$

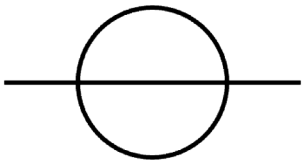

FIG. 13. Melon diagram proportional to λ_C.

From the cyclic property, all ways of contraction can be written as

$$8\times 4\times\frac{1}{2!}\left(\frac{g_C^2}{2}\right)^2\sum_{b,c,d,e}\overbracket{a(bcbc)(dede)}a \tag{C36}$$

where 8 is because of eight X's in $bcbcdede$ and 4 is because of four X's in $dede$. From this, there is only one way to contract in the leading order as

$$8\times 4\times \overbracket{a\overbracket{(bcbc)\overbracket{(dede)}}a}\,. \tag{C37}$$

Therefore, the coefficient is

$$8\times 4\times\frac{1}{2!}\left(\frac{g_C^2}{2}\right)^2\times N^2 D = 4\frac{(\lambda_C D)^2}{D}. \tag{C38}$$

Thus,

$$c_C = 4. \tag{C39}$$

[1] T. Banks, W. Fischler, S. H. Shenker, and L. Susskind, M theory as a matrix model: A conjecture, Phys. Rev. D **55**, 5112 (1997).

[2] I. R. Klebanov, F. Popov, and G. Tarnopolsky, TASI lectures on large N tensor models, Proc. Sci., TASI2017 (**2018**) 004 [arXiv:1808.09434].

[3] F. Ferrari, The large D limit of planar diagrams, Ann. Inst. Henri Poincare **6**, 427 (2019).

[4] T. Azeyanagi, F. Ferrari, and F. I. Schaposnik Massolo, Phase diagram of planar matrix quantum mechanics, tensor, and Sachdev-Ye-Kitaev models, Phys. Rev. Lett. **120**, 061602 (2018).

[5] T. Hotta, J. Nishimura, and A. Tsuchiya, Dynamical aspects of large N reduced models, Nucl. Phys. **B545**, 543 (1999).

[6] G. Mandal, M. Mahato, and T. Morita, Phases of one dimensional large N gauge theory in a $1/D$ expansion, J. High Energy Phys. 02 (2010) 034.

[7] N. Kolganov and D. A. Trunin, Classical and quantum butterfly effect in nonlinear vector mechanics, Phys. Rev. D **106**, 025003 (2022).

[8] D. Stanford, Many-body chaos at weak coupling, J. High Energy Phys. 10 (2016) 009.
[9] J. D. Bjorken and S. D. Drell, *Relativistic Quantum Mechanics*, International Series in Pure and Applied Physics (McGraw-Hill, New York, 1965), see Secs. 19.2 and 19.3.
[10] C. D. Roberts and A. G. Williams, Dyson-Schwinger equations and their application to hadronic physics, Prog. Part. Nucl. Phys. **33**, 477 (1994).
[11] L. von Smekal, A. Hauck, and R. Alkofer, A solution to coupled Dyson-Schwinger equations for gluons and ghosts in Landau gauge, Ann. Phys. (N.Y.) **267**, 1 (1998); **269**, 182 (E) (1998).
[12] D. N. Kabat and G. Lifschytz, Approximations for strongly coupled supersymmetric quantum mechanics, Nucl. Phys. **B571**, 419 (2000).
[13] R. D. Pisarski, Computing finite temperature loops with ease, Nucl. Phys. **B309**, 476 (1988).
[14] R. R. Parwani, Resummation in a hot scalar field theory, Phys. Rev. D **45**, 4695 (1992); **48**, 5965(E) (1993).
[15] M. Laine and A. Vuorinen, *Basics of Thermal Field Theory*, Lecture Notes in Physics Vol. 925 (Springer, Cham, 2016).
[16] G. Cuniberti, E. De Micheli, and G. A. Viano, Reconstructing the thermal Green functions at real times from those at imaginary times, Commun. Math. Phys. **216**, 59 (2001).
[17] N. Iizuka, D. N. Kabat, G. Lifschytz, and D. A. Lowe, Probing black holes in nonperturbative gauge theory, Phys. Rev. D **65**, 024012 (2002).
[18] N. Iizuka and J. Polchinski, A matrix model for black hole thermalization, J. High Energy Phys. 10 (2008) 028.
[19] B. Michel, J. Polchinski, V. Rosenhaus, and S. J. Suh, Four-point function in the IOP matrix model, J. High Energy Phys. 05 (2016) 048.
[20] N. Iizuka and M. Nishida, Out-of-time-ordered correlators in the IP matrix model, J. High Energy Phys. 05 (2024) 026.
[21] A. Zee, *Quantum Field Theory in a Nutshell* (Princeton University Press, Princeton, NJ, 2003), p. 192.